

# Auto-encoding graph-valued data with applications to brain connectomes

Meimei Liu\*, Zhengwu Zhang†, David B. Dunson‡

## Abstract

Our interest focuses on developing statistical methods for analysis of brain structural connectomes. Nodes in the brain connectome graph correspond to different regions of interest (ROIs) while edges correspond to white matter fiber connections between these ROIs. Due to the high-dimensionality and non-Euclidean nature of the data, it becomes challenging to conduct analyses of the population distribution of brain connectomes and relate connectomes to other factors, such as cognition. Current approaches focus on summarizing the graph using either pre-specified topological features or principal components analysis (PCA). In this article, we instead develop a nonlinear latent factor model for summarizing the brain graph in both unsupervised and supervised settings. The proposed approach builds on methods for hierarchical modeling of replicated graph data, as well as variational auto-encoders that use neural networks for dimensionality reduction. We refer to our method as Graph AuTo-Encoding (GATE). We compare GATE with tensor PCA and other competitors through simulations and applications to data from the Human Connectome Project (HCP).

**Keywords:** Brain networks; Dimensionality reduction; Graph data; Non-linear factor analysis; Neuroscience; Replicated networks; Variational Auto-encoder.

## 1 Introduction

Understanding the brain connectome and how it relates to human traits and various clinical variables has drawn huge attention recently [1, 2, 3, 4], and has motivated large neuroimaging studies with thousands of subjects, such as the UK Biobank [5], the Human Connectome Project (HCP) [6], and the Adolescent Brain Cognitive Development cohort [7]. Through these studies, there have been

---

\*Postdoc, Department of Statistical Science, Duke University, Durham, NC, 27705. E-mail: meimei.liu@duke.edu.

†Assistant Professor, Department of Biostatistics and Computational Biology, University of Rochester E-mail: zhengwu\_zhang@urmc.rochester.edu.

‡Professor, Department of Statistical Science, Duke University E-mail: dunson@duke.edu.

dramatic improvements in ability to reconstruct brain connectomes thanks to advanced hardware [8], novel image acquisition protocols [8, 9], and new reconstruction algorithms [10, 11]. Inspired by these developments, we are interested in creating advanced analysis methods for the brain structural connectome recovered from diffusion MRI data. It is important to obtain parsimonious representations of the connectome via accurate embeddings in Euclidean space, while using such embeddings to link brain function and human behavior. Let  $A_i$  represent the structural connectivity recovered from subject  $i$ , whose elements  $A_{i[uv]}$  characterize white matter connection properties between different brain regions  $u$  and  $v$ . Such data can be considered as a type of *replicated graph* [12]. A fundamental challenge in analyzing replicated graphs is how to appropriately summarize each individual graph in a parsimonious manner, isolating unique features of that graph while maintaining an ability to study similarities and differences across graphs.

There is an immense literature focused on analysis of a single graph, ranging from simple Erdos-Renyi and stochastic block characterizations to more elaborate mixed-membership stochastic block [13] and latent space models [14]. However, the literature on replicated graphs is still in its infancy. Based on a latent space characterization, Durante et al. ([15]) proposed a random effects model to characterize the population distribution of a set of binary networks. Their model incorporated a component characterizing the average graph, while modeling individual-specific deviations using a low-rank structure. By using a Dirichlet process prior for the distribution of the individual-specific random effects, the model induces clustering of individuals and allows inference on group differences according to their brain structure [16]. There are also papers on optimization-based factorization approaches for replicated graphs. One approach is to simply stack the adjacency matrices for each individual into a tensor, and then apply tensor PCA and its variants to get summary scores of networks ([17] and [18]). These scores are treated as surrogates of networks in subsequent analyses, e.g., relating brain networks to human traits ([17]).

Although Durante et al ([15]) provide a flexible representation of the population distribution of replicated graphs, their approach relies on a computationally intensive Bayesian analysis with Markov chain Monte Carlo. The tensor PCA method is relatively efficient computationally and provides a simple low-dimensional summary of an individual’s brain structure, but it does not allow inference on the population distribution. Moreover, these PCA-based methods are all linear methods, which may have limited ability to parsimoniously represent the non-Euclidean structure in the complex graph data. A major motivation of this article is to develop a nonlinear latent factor modeling approach that provides a characterization of the population distribution of brain graphs, while also outputting a low-dimensional vector of features that can be used to summarize an individual’s graph, facilitating prediction and inference.

With this motivation, we are particularly intrigued by recent developments in the machine learning

literature using neural networks for non-linear dimensionality reduction. Generative algorithms such as Variational Auto-Encoders (VAEs) [19], [20], have proven successful in representing images via low dimensional latent variables, which are incorporated within a deep neural network. VAEs model the population distribution of image data through a simple distribution for the latent variables combined with a complex non-linear mapping function. In the imaging context, a key to the success of such methods is the use of convolutional operators to encode symmetries often present in imaging data. However, replicated graph data have a fundamentally different geometric structure and such methods cannot be employed directly.

We develop a model-based variational **Graph Auto-Encoder** (GATE). The GATE approach has two important components: (1) a nonlinear latent factor model to obtain a low-dimensional representation of individual network  $A_i$ , denoted as  $z_i$ ; and (2) a hierarchical generative model designed to learn the population conditional distribution  $p(A_i|z_i)$ . We model each cell  $A_{i[uv]}$  in  $A_i$  using a latent space model [14], with the latent coordinates of the regions  $u$  and  $v$  varying as a nonlinear function of the individual-specific features  $z_i$ . Two layers of nonlinear dimensionality reduction for replicated graphs are achieved in GATE: one on the individuals to reduce dimensionality in characterizing differences among individuals, and one on the nodes to reduce dimensionality in characterizing the network structure within each individual in the style of latent space models for networks.

For node dimensionality reduction, we utilize a graph convolutional neural network (GCN) to incorporate the geometric structure of the brain graphs and employ a nonlinear function to learn the latent representation of the regions. Convolutional neural networks are effective architectures in image and audio recognition tasks [21] [22] [23], thanks to their ability to exploit the local translational invariance structures over their domain. GCN is an extension of convolutional neural networks (CNN) that enables automatic feature extraction and summarization for graph-based data. The major GCN methods include spectral-based approaches [24] that rely on the eigen-decomposition of the graph Laplacian matrix, and spatial-based approaches that aggregate feature information from neighbors [25]. Existing GCN approaches either focus on the node-level embedding of a single graph [25], [26] with applications in link prediction, or provide a compact representation of the graph itself [27], [28] with applications including graph classification tasks.

However, directly applying current GCN methods to learn the regions' representation for replicated graphs is problematic without fully considering the following distinct features of the brain structural networks: (1) sparsity, implying the regions are not fully connected; (2) transitivity, implying that region  $u$  and  $v$  being connected to the same region suggests that  $u$  and  $v$  are not far away in the latent representation space; (3) distinction, meaning each region has a distinct collaborative pattern to its neighbors; (4) similarity, implying each subject has shared structures

with others but also maintains its unique set of features. Figure 1 displays the structural connectivity pattern in one young adult human brain. Inspired by the unique structure of the human brain, we develop a novel graph convolutional network (GCN) in GATE to obtain low-dimensional region representations, while fully exploiting the above features. More specifically, since brain gray matter regions (those ROIs in Figure 1 (c)) are connected through white matter tracts, the distance between each pair of regions is controlled by these anatomical connections. Our proposed GCN naturally accommodates such intrinsic properties as part of the geometric structure, and learn the region’s representation by propagating region-specific  $k$ -nearest neighbor information.

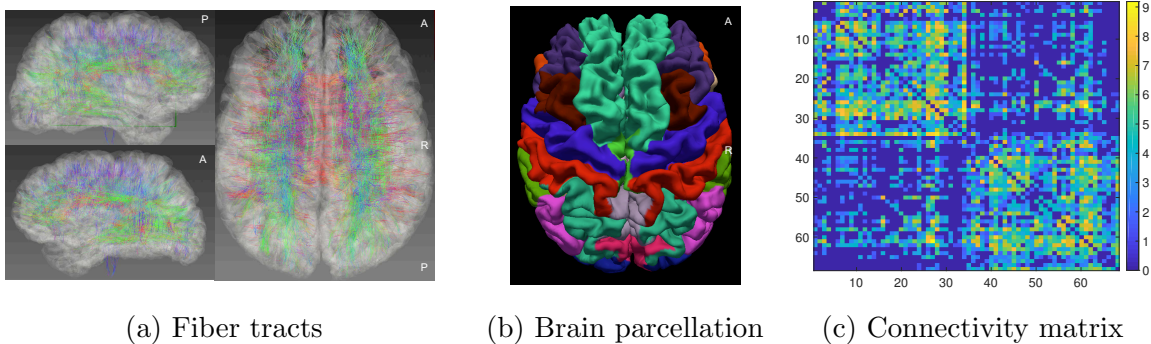


Figure 1: One example of brain structural connectivity. (a) subsampled white matter fiber tracts in one person’s brain; (b) an anatomical parcellation of the brain into different regions of interest (ROIs), coded by color; and (c) a connectivity matrix generate using data in (a) and (b).

We further extend GATE to relate human phenotypes with brain structural connectivity, which we refer to as **regression with GATE** (reGATE). reGATE is a supervised embedding method that simultaneously learns the population distribution, graph representations and a predictive model, avoiding training two separate objective functions. We highlight that the resulting graph representations in reGATE are more interpretable in the sense that a linear relationship between the individual-specific features  $z_i$  and a human trait is characterized. reGATE can simulate high dimensional brain graphs with desired human trait information. This is advantageous particularly in learning how graph connectivity varies with the human trait of interest.

We remark that few attempts have been made to integrate regression models into the VAE framework. The typical strategy applies unsupervised VAE as a first stage, and then uses the resulting features in a regression; see [29] as an example. [30] and [31] directly build the regression on the original data without employing low dimensional features, and hence are infeasible in high dimensional cases.

The paper is organized as follows. In Section 2 we introduce background on the latent space model, and describe our proposed GATE approach. In Section 3 we develop supervised reGATE.

Section 4 contains a simulation study showing advantages of GATE and reGATE relative to competitors. In Section 5 we apply GATE and reGATE to human brain network data from the Human Connectome Project (HCP).

## 2 The Graph Auto-Encoder Model

Denote the brain network data from subject  $i$  ( $i = 1 \dots, n$ ) as  $\mathcal{G}_i = (\mathcal{V}, E_i)$  with  $\mathcal{V} = (1, \dots, V)$  representing a set of nodes (i.e., brain regions) and  $E_i$  representing connectivity patterns between the nodes. In our application, we assume the  $\mathcal{V}$  are registered across the population, i.e., each node represents the same brain region across different subjects. We can represent  $\mathcal{G}_i = (\mathcal{V}, E_i)$  as a  $V \times V$  symmetric adjacency matrix  $A_i$ , where  $A_{i[uv]}$  is used to denote the connection weight between nodes  $u$  and  $v$ , and  $A_{i[uu]} = 0$  since we do not consider self-relationships. We consider the fiber count feature for  $A_{i[uv]}$ , which will be 0 or a positive integer. For notation simplicity, we will also use

$$L(A_i) = (A_{i[21]}, A_{i[31]}, \dots, A_{i[V1]}, A_{i[32]}, \dots, A_{i[V2]}, \dots, A_{i[V(V-1)]})$$

to denote the lower triangular elements of matrix  $A_i$ . In addition to  $\mathcal{G}$ , we also observe covariate  $y_i$  for each subject, measuring cognition or other traits.

### 2.1 Latent space model for replicated graphs

Latent space models [14] provide a probabilistic framework that assumes the edges in the networks are conditionally independent given their corresponding edge probabilities, with these probabilities defined as a function of pairwise distances between the nodes in a latent space. Latent space models can flexibly characterize variability across individuals in brain connectivity, while accommodating the complexity of network structures within each individual. Borrowing the conditional independence idea of latent space models, we assume that the connection strengths between brain regions are conditionally independent Poisson variables, given a subject-specific Poisson rate vector  $\lambda_i = \{\lambda_{i1}, \dots, \lambda_{iV(V-1)/2}\}^\top$ ,

$$A_{i\ell} | \lambda_{i\ell} \sim \text{Poisson}(\lambda_{i\ell}), \tag{2.1}$$

independently for each pair  $\ell = 1, \dots, V(V-1)/2$  and  $i = 1, \dots, n$ . We assume  $\log(\lambda_{i\ell})$  has the following factorization form:

$$\log(\lambda_{i\ell}) = \gamma_\ell + \psi_\ell^{(i)}, \tag{2.2}$$

$$\psi_\ell^{(i)} = \sum_{r=1}^R \alpha_r X_{ur}^{(i)} X_{vr}^{(i)}, \quad \text{for } \ell = [uv], \tag{2.3}$$

$$\text{and } X_r^{(i)} = (X_{1r}^{(i)}, \dots, X_{Vr}^{(i)})^\top. \tag{2.4}$$

As shown in (2.2),  $\log(\lambda_{il})$  is decomposed into two parts: a baseline parameter  $\gamma_\ell$  controlling connection strength between the  $\ell$ th pair of brain regions, representing shared structure across individuals, and an individual deviation  $\psi_\ell^{(i)}$ . Taking into account symmetry constraints and excluding the diagonal elements, there are  $V(V-1)/2$  unknown  $\{\lambda_{il}\}$  for each subject, leading to a daunting dimensionality problem. To reduce dimensionality, [15] proposed to use a SVD-type latent factorization, as shown in (2.3), where  $r = 1, \dots, R$  indexes the different latent dimensions,  $\alpha_r > 0$  is a weight on the importance of the dimension  $r$ , and  $X_{ur}^{(i)}$  is the  $r$ th latent factor specific to brain region  $u$  and subject  $i$ . According to (2.3-2.4), if  $X_{ur}^{(i)}$  and  $X_{vr}^{(i)}$  have the same sign and neither are close to zero, we have  $X_{ur}^{(i)}X_{vr}^{(i)} > 0$  and there will be a positive increment on  $\psi_\ell^{(i)}$  and hence on the expectation of the connection strength for the  $\ell = (u, v)$  connection of subject  $i$ .

For replicated graphs, we face many challenges in learning the latent representations using existing latent space models: (1) Non-linearity: graph data are generally non-Euclidean with complicated structures. Designing a model to efficiently capture the non-linear structure is difficult. (2) Sparsity: brain regions are not fully connected, especially the structural brain networks considered in this paper. (3) Speed: existing latent space approaches often rely on Markov chain Monte Carlo sampling, which is computationally intensive for high dimensional graphs. It is desirable to develop a fast “nonlinear” factorization model for large scale neuroimaging data analysis. To address these challenges, we propose an autoencoder-based approach called Graph Autoencoder (GATE), from which we model the latent coordinates  $X_u^{(i)}$  as a nonlinear function of a lower-dimensional vector  $z_i$ , which serves as a low-dimensional representation of  $A_i$ .

## 2.2 The Graph AutoEncoder (GATE) Model

GATE relies on the variational autoencoder (VAE) which is a popular technique for non-linear dimension reduction. In studying replicated graphs, a VAE usually consists of two components. The first component is a generative model that specifies how the latent variables  $z_i$  give rise to the observations  $A_i$  through a nonlinear mapping, parametrized by neural networks. The second component is an inference model that learns the inverse mapping from  $A_i$  to  $z_i$ . In the following context, we frame our proposed Graph Autoencoder (GATE) method using the same terminology as in the VAE literature.

### 2.2.1 Generative model

Denote  $z_i \in \mathbb{R}^K$  as a low-dimensional latent representation of the graph  $A_i$ . For each subject  $i$ , we assume  $A_{i\ell}$  for  $\ell = 1, \dots, V(V-1)/2$  are conditionally independent given the latent representation

$z_i$ . Therefore, the likelihood of  $L(A_i)$  is

$$p_\theta(L(A_i) = a_i|z_i) = \prod_{\ell=1}^{V(V-1)/2} p_\theta(A_{i\ell} = a_{i\ell}|z_i). \quad (2.5)$$

$p_\theta(A_{i\ell}|z_i)$  is a generative model for the weighted adjacency matrix  $A_i$  given the latent  $z_i$  with  $z_i \sim p(z)$ . We define  $p(z) = N(0, I_k)$ , representing all observed connectomes in the same Gaussian latent space; we learn the mapping from the Gaussian latent space to the complex observation distribution by a complicated function via a deep neural network equipped with parameters  $\theta$ .

Specifically, we assume the observations  $A_{i\ell}$  arise from the following generative process:

$$\begin{aligned} z_i &\sim N(0, I_K), \\ A_{i\ell}|z_i &\sim \text{Poisson}(\lambda_{i\ell}(z_i)), \end{aligned} \quad (2.6)$$

where  $\ell = [uv]$  indexes the connection between the  $u$ -th and  $v$ -th brain regions, and the Poisson rate parameter  $\lambda_{i\ell}(z_i)$  is modeled as a nonlinear function of  $z_i$  according to:

$$\lambda_{i\ell}(z_i) = \exp(\gamma_\ell + \psi_\ell(z_i)), \quad (2.7)$$

$$\psi_\ell(z_i) = \sum_{r=1}^R \alpha_r X_{ur}(z_i) X_{vr}(z_i), \quad \text{for } \ell = [uv], \quad (2.8)$$

$$X_r(z_i) = (X_{1r}(z_i), \dots, X_{Vr}(z_i))^\top = g_r(z_i), \quad (2.9)$$

where  $g_r(\cdot) : \mathbb{R}^K \rightarrow \mathbb{R}^V$  is a nonlinear mapping from  $z_i$  to the  $r$ th latent factor of the brain regions  $X_r$ , parameterized by deep neural networks with parameters  $\theta$  for  $r = 1, \dots, R$ .

When the elements  $A_{i\ell} \in \{0, 1\}$  are binary instead of counts, we instead let

$$A_{i\ell}|z_i \sim \text{Binomial}(\lambda_{i\ell}(z_i)), \quad \text{with } \lambda_{i\ell}(z_i) = \frac{e^{\gamma_\ell + \psi_\ell(z_i)}}{1 + e^{\gamma_\ell + \psi_\ell(z_i)}}, \quad (2.10)$$

and  $\psi_\ell(z_i)$  following the same factorization as in equations (2.8)-(2.9).

Denote  $\mathbf{X}(z_i) = (X_1(z_i), \dots, X_R(z_i)) \in \mathbb{R}^{V \times R}$ . The  $u$ -th row  $(X_{u1}(z_i), \dots, X_{uR}(z_i))$  represents the latent features of the region  $u \in \mathcal{V}$ . A relatively large positive value for the cross product between the  $u$ -th and  $v$ -th rows implies a relatively high connection strength between these brain regions. Each column  $X_r(z_i)$  can be considered as an ‘‘image’’ with each region as an irregular pixel; and we have  $R$  such ‘‘images’’ for each individual. Convolutional neural networks are highly effective architectures in image and audio recognition tasks [21] [22] [23], thanks to their ability to exploit the local translational invariance structures over their domain. Considering the unique features of the brain connectome networks, we aim to generalize the CNN and define appropriate graph convolutions to learn the nonlinear mapping  $\{g_r(\cdot)\}$  via exploiting the local collaborative pattern.



We leverage the intrinsic locality of structural brain networks, and propose a novel graph convolutional network (GCN) to learn each region’s representation by propagating node-specific  $k$ -nearest neighbor information. The intrinsic locality here refers to the relative distance between brain regions measured through the length of white matter fiber tracts connecting them. We extract this information from brain imaging tractography and store it in a matrix  $B \in \mathbb{R}^{V \times V}$ , where  $B_{uv}$  is the averaged length of fiber tracts between region  $u$  and  $v$ ,  $B_{uv} = B_{vu}$ ,  $B_{uu} = 0$ , and we set  $B_{uv} = \infty$  if there are no fibers between them. For each region  $u$ , we define its  $k$ -nearest neighbors ( $k$ -NN( $u$ )) as the  $k$  ROIs closest to  $u$  according to our notion of distance, and denote the region itself as its 0-NN.

To learn the  $r$ -latent coordinate  $g_r(z_i)$  for subject  $i$ , we define an  $M$ -layer GCN as follows:

$$X_r^{(i,1)} = h_1(W^{(r,1)}z_i + b_1), \quad (2.11)$$

$$X_r^{(i,m)} = h_m(W^{(r,m)}X_r^{(i,m-1)} + b_m) \quad \text{for } 2 \leq m \leq M, \quad (2.12)$$

where  $X_r^{(i,m)}$  denotes the output of the  $m$ -th layer of the convolutional neural network,  $h_m(\cdot)$  is an activation function for the  $m$ th layer, and  $W^{(r,m)}$  is the weight matrix that characterizes the convolutional operator at this layer. We denote the parameters  $b_m$ ,  $W^{(r,m)}$ , together with  $\gamma_\ell$ ,  $\alpha_r$  in (2.7-2.8) ( $m = 1, \dots, M, r = 1, \dots, R, \ell = 1, \dots, V(V-1)/2$ ) as the model parameter  $\theta$ . The activation functions  $\{h_m(\cdot)\}$  can be chosen from the following candidates based on the performance: (1) rectified linear unit (ReLU) function, which is widely used [32] in deep neural networks, with the definition as  $ReLU(x) = \max(0, x)$ , where the max operation is applied element-wise; (2) Sigmoid function defined as  $h_m(x) = \frac{1}{1+e^{-x}} \in (0, 1)$ ; (3) linear or identity function  $h_m(x) = ax$  with  $a \neq 0$ .

For  $m = 1$ ,  $W^{(r,1)} \in \mathbb{R}^{V \times K}$  maps the latent representation  $z_i \in \mathbb{R}^K$  to the latent space  $X_r^{(i,1)} \in \mathbb{R}^{V \times 1}$ ; for  $m \geq 2$ ,  $W^{(r,m)}$  is a  $V \times V$  weight matrix with the  $u$ -th row  $w_u^{(r,m)}$  satisfying  $w_{uv}^{(r,m)} > 0$  if  $v = u$  or  $v \in k_r$ -NN( $u$ ), and  $= 0$  otherwise. (2.12) implies that the embedding feature of each region at the  $m$ -th layer is determined by the weighted sum of itself and its nearest neighbor regions at the  $(m-1)$ -th layer; and the related weights aim to characterize the region-specific local connectivity. For  $r = 1, \dots, R$ , we can choose different values of  $k$  to define its  $k_u$ -NN to fully explore the possible collaboration patten among brain regions.

Figure 2 shows how a three-layer GCN learns  $X_r(z_i)$  via a 2-NN GCN. First, we initialize the latent feature for each region as  $x_{ur}^{(i,1)}$  based on (2.11). Then, we construct a “graph” based on the fiber length in  $B$ : each region is assigned to connect with 2 nearest neighbors at most according to its connection strength (fiber length) to other brain regions. Note that if a region  $u$  has less than  $k = 2$  direct neighbors, we will include all the regions  $v$  satisfying  $B_{uv} \in (0, \infty)$  as its neighbors. This information is reflected in  $W^{(i,m)}$ , whose rows only contain at most 3 non-zero elements (one at the diagonal and two off the diagonal). Next, we update the latent feature of each region in the



next layer based on a sum of reweighted features from its 2 nearest neighbors and itself.

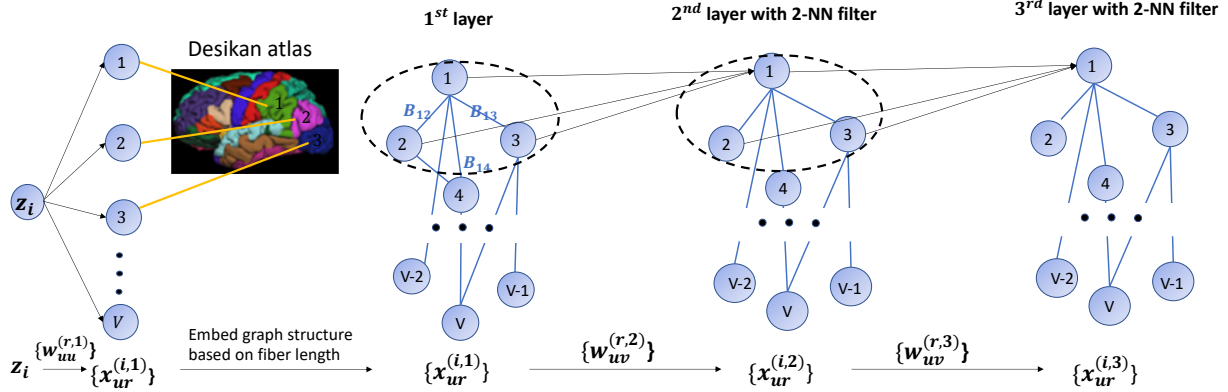


Figure 2: Illustrative example of three-layer GCN architecture with 2-NN filters. For example, for node 1, the 2-NN is node 2 and node 3.  $x_{1r}^{(i,1)} = h_1(w_{11}^{(r,1)} z_i)$ ,  $x_{1r}^{(i,2)} = h_2(w_{11}^{(r,2)} x_{1r}^{(i,1)} + w_{12}^{(r,2)} x_{2r}^{(i,1)} + w_{13}^{(r,2)} x_{3r}^{(i,1)})$ .

## 2.2.2 Variational Inference and the GATE Learning

To train and evaluate the deep generative model in (2.6), we are interested in estimating  $\theta$ , the parameters characterizing the mapping from  $z_i$  to  $A_{il}$ , and  $p_\theta(z_i|A_i)$ , the posterior distribution of the latent variable. By applying Bayes rule, we have the posterior as

$$p_\theta(z_i|A_i) = \frac{p_\theta(A_i|z_i)p(z_i)}{p_\theta(A_i)}.$$

Since the likelihood function  $p_\theta(A_i|z_i)$  is parameterized via the neural network with non-linear transformations, both the marginal distribution  $p_\theta(A_i)$  and the posterior probability distribution  $p_\theta(z_i|A_i)$  are intractable. Hence, we resort to variational inference (VI) ([33], [34]), a widely-used tool for approximating intractable posterior distributions. VI provides an alternative strategy to Markov chain Monte Carlo (MCMC) sampling by replacing sampling with an optimization problem. VI seeks a simple distribution  $q_\phi(z_i|A_i)$  parameterized by  $\phi$  from a variational family, e.g., a Gaussian distribution family, that best approximates  $p_\theta(z_i|A_i)$ . We call such  $q_\phi(z_i|A_i)$  as the probabilistic encoder, which maps the input  $A_i$  to a low dimensional latent representation  $z_i$ . The approximated posterior  $q_\phi(z_i|A_i)$  should be close to  $p_\theta(z_i|A_i)$ . We use Kullback-Leibler (KL) divergence to quantify the distance between these two distributions, which is defined as  $D_{KL}(Q||P) = E_{z \sim Q} \log \frac{Q(z)}{P(z)}$ , measuring how much information is lost if the distribution  $Q$  is used to represent  $P$ .

Here we set  $q_\phi(z_i|A_i)$  to be a fully factorized (diagonal) Gaussian distribution with mean  $\mu_\phi(A_i)$  and covariance  $\text{diag}\{\sigma_\phi^2(A_i)\}$ , with deep neural networks designed to learn the parameter  $\phi$ .

Particularly, we learn  $\mu_\phi$  and  $\sigma_\phi^2$  via

$$\begin{aligned} \mu_\phi(A_i) &= \varphi_{N,\mu}[W_{N,\mu}\varphi_{N-1,\mu}\{W_{N-1,\mu}\cdots\varphi_{1,\mu}(W_{1,\mu}A_i + b_{1\mu}) + b_{N-1,\mu}\} + b_{N,\mu}], \\ \text{diag}\{\sigma_\phi^2(A_i)\} &= \text{diag}\{\varphi_{N,\sigma}[W_{N,\sigma}\varphi_{N-1,\sigma}\{W_{N-1,\sigma}\cdots\varphi_{1,\sigma}(W_{1,\sigma}A_i + b_{1\sigma}) + b_{N-1,\sigma}\} + b_{N,\sigma}]\}, \end{aligned} \quad (2.13)$$

where  $b_{i,\mu}, W_{i,\mu}, b_{i,\sigma}, W_{i,\sigma}$  for  $i = 1, \dots, N$  are weights within the deep neural networks,  $N$  is the number of layers that determine the models learning capacity, and  $\{\varphi_{i,\mu}\}$  and  $\{\varphi_{i,\sigma}\}$  are activation functions that will be specified later. We denote these weights and activation functions together as the parameter  $\phi$ .

We aim to maximize the log-likelihood of generating data, i.e.,  $\log p_\theta(A_i)$ , and also minimize the difference between the true posterior  $p_\theta(z_i|A_i)$  and approximated posterior distribution  $q_\phi(z_i|A_i)$ . Note that

$$\begin{aligned} D_{KL}(q_\phi(z_i|A_i)||p_\theta(z_i|A_i)) &= \int q_\phi(z_i|A_i) \log \frac{q_\phi(z_i|A_i)}{p_\theta(z_i|A_i)} dz_i = \int q_\phi(z_i|A_i) \log \frac{q_\phi(z_i|A_i)p_\theta(A_i)}{p_\theta(A_i|z_i)p_\theta(z_i)} dz_i \\ &= \log p_\theta(A_i) + D_{KL}(q_\phi(z_i|A_i)||p_\theta(z_i)) - \mathbb{E}_{q_\phi(z_i|A_i)}(\log p_\theta(A_i|z_i)). \end{aligned}$$

Then we have

$$\begin{aligned} &\log p_\theta(A_i) - D_{KL}(q_\phi(z_i|A_i)||p_\theta(z_i|A_i)) \\ &= \mathbb{E}_{q_\phi(z_i|A_i)}[\log p_\theta(A_i|z_i)] - D_{KL}(q_\phi(z_i|A_i)||p_\theta(z_i)) := -\mathcal{L}(A_i; \theta, \phi). \end{aligned} \quad (2.14)$$

Since  $D_{KL}(q_\phi(z_i|A_i)||p_\theta(z_i|A_i))$  is nonnegative,  $-\mathcal{L}(A_i; \theta, \phi)$  is a lower bound on the marginal log-likelihood, referred to as the evidence lower bound (ELBO), which is a function of both  $\theta$  and  $\phi$ . Therefore, the training objective is minimizing the negative of the ELBO, i.e., minimizing

$$\mathcal{L}(A_i; \theta, \phi) = -\mathbb{E}_{q_\phi(z_i|A_i)}[\log p_\theta(A_i|z_i)] + D_{KL}(q_\phi(z_i|A_i)||p_\theta(z_i)). \quad (2.15)$$

$\mathcal{L}(A_i; \theta, \phi)$  consists of two parts: the first term is the reconstruction error, that measures how well the model can reconstruct  $A_i$ ; while the second term, defined as the KL divergence between the approximate posterior from the prior, is a regularizer that pushes  $q_\phi(z_i|A_i)$  to be as close as possible to its prior  $N(0, 1)$  so that we can sample it easily.

However, the expectation in the ELBO is intractable. To address this, we employ Monte Carlo variational inference [19] by approximating the troublesome expectation with samples of the latent variables from the variational distribution  $z_i \sim q_\phi(z_i|A_i)$ . Particularly, we form the Monte Carlo estimates of the expectation as

$$\mathbb{E}_{q_\phi(z_i|A_i)}[\log p_\theta(A_i|z_i)] \simeq \frac{1}{L} \sum_{\ell=1}^L \log p_\theta(A_i|z_i^\ell),$$

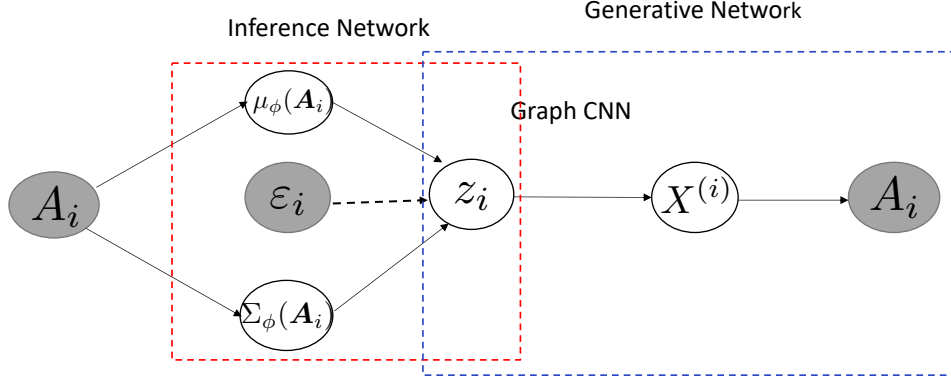


Figure 3: A taxonomy of GATE. The dashed line with an arrow denotes a sampling operation.

where  $z_i^\ell$  is sampled with the reparametrization trick: sampling  $\varepsilon_i^\ell \sim N(0, I_K)$  and reparametrizing  $z_i^\ell = \mu_\phi(A_i) + \varepsilon_i^\ell \odot \Sigma_\phi(A_i)$ , where  $\Sigma_\phi(A_i) = \text{diag}\{\sigma_\phi^2(A_i)\}$ . Simple calculation shows that the KL-divergence  $D_{KL}(q_\phi(z_i|A_i)||p(z_i)) = \frac{1}{2} \sum_{k=1}^K (\mu_k^2 + \sigma_k^2 - 1 - \log(\sigma_k^2))$ , where  $\mu_k$  and  $\sigma_k$  are the  $k$ -th element of  $\mu_\phi(A_i)$  and  $\Sigma_\phi(A_i)$  respectively. Therefore, the ELBO in (2.15) can be approximated as

$$\mathcal{L}(A_i; \theta, \phi) \simeq \tilde{\mathcal{L}}(A_i; \theta, \phi) = -\frac{1}{L} \sum_{\ell=1}^L \log p_\theta(A_i|z_i^\ell) + \frac{1}{2} \sum_{k=1}^K (\mu_k^2 + \sigma_k^2 - 1 - \log(\sigma_k^2)),$$

which are differentiable with respect to  $\theta$  and  $\phi$ . Then, given  $n$  observed networks, we can construct an estimator of the ELBO of the full dataset, based on the minibatches  $\frac{n}{m} \sum_{i=1}^m \tilde{\mathcal{L}}(A_{(i)}; \theta, \phi)$ , where  $\{A_{(i)}\}_{i=1}^m$  is a randomly drawn sample of size  $m$  from the full observed data with sample size  $n$ .

Viewing  $\frac{n}{m} \sum_{i=1}^m \tilde{\mathcal{L}}(A_{(i)}; \theta, \phi)$  as the objective, we implement a stochastic variational Bayesian algorithm to optimize  $\theta$  and  $\phi$ , respectively. Figure 3 shows the graphical diagram of the GATE approach; Algorithm 1 summarizes the GATE training procedure.

### 3 Regression with GATE and Inference

#### 3.1 Regression GATE for predicting human traits

In addition to finding low-dimensional representations of brain structure networks, we also are interested in inferring the relationship between brain networks and human traits, such as cognition. With this goal in mind, we develop a supervised version of GATE referred to as regression GATE (reGATE). Let  $y_i$  be the trait of the  $i$ -th subject. The joint log likelihood of  $(A_i, y_i)$  can be expressed

---



---

**Input:**  $\{A_i\}_{i=1}^n, \{z_i\}_{i=1}^n$ , geometric matrix  $B$ , mini-batch size  $m$ , latent space dimension  $R$ .

---

Randomly initialize  $\theta, \phi$

**while** not converged **do**

    Sample a batch of  $\{A_i\}$  with size  $m$ , denote as  $A_{(i)}$  for  $i = 1, \dots, m$ .

**for all**  $A_i \in \mathcal{A}_m$  **do**

        Sample  $\varepsilon_i \sim N(0, I_R)$ , and compute  $z_i = \mu_\phi(A_i) + \varepsilon_i \odot \Sigma_\phi(A_i)$ .

        Compute the gradients  $\nabla_\theta \tilde{\mathcal{L}}(A_{(i)}; \theta, \phi)$  and  $\nabla_\phi \tilde{\mathcal{L}}(A_{(i)}; \theta, \phi)$  with  $z_i$ .

    Average the gradients across the batch.

    Update  $\theta, \phi$  using gradients of  $\theta, \phi$ .

**Return**  $\theta, \phi$ .

---



---

Table 1: Training GATE model using gradients.

as

$$\begin{aligned}
\log p_\theta(A_i, y_i) &= \mathbb{E}_{q_\phi(z_i|A_i)} \log \frac{p_\theta(A_i, z_i)p_\theta(y_i|A_i, z_i)}{p_\theta(z_i|A_i, y_i)} \\
&= \mathbb{E}_{q_\phi(z_i|A_i)} \log \frac{p_\theta(A_i|z_i)p_\theta(z_i)p_\theta(y_i|z_i)q_\phi(z_i|A_i)}{q_\phi(z_i|A_i)p_\theta(z_i|y_i, A_i)} \\
&= \mathbb{E}_{q_\phi(z_i|A_i)} \log p_\theta(y_i|z_i) + \mathbb{E}_{q_\phi(z_i|A_i)} \log p_\theta(A_i|z_i) - D_{KL}(q_\phi(z_i|A_i)||p_\theta(z_i)) \\
&\quad + D_{KL}(q_\phi(z_i|A_i)||p_\theta(z_i|y_i, A_i)) \\
&= -\mathcal{L}(A_i, y_i; \theta, \phi) + D_{KL}(q_\phi(z_i|A_i)||p_\theta(z_i|y_i, A_i)), \tag{3.1}
\end{aligned}$$

where we have  $p_\theta(y_i|A_i, z_i) = p_\theta(y_i|z_i)$  since we assume the human trait  $y_i$  and the brain connectivity  $A_i$  are conditionally independent given the latent representation  $z_i$  for the  $i$ -th subject; see Figure 4 for an illustration of the model. In (3.1), we divide the log-likelihood of  $(A_i, y_i)$  into two parts: the ELBO denoted as  $-\mathcal{L}(A_i, y_i; \theta, \phi)$ , and the non-negative KL-divergence between  $q_\phi(z_i|A_i)$  and  $p_\theta(z_i|y_i, A_i)$ . Different from the unsupervised ELBO in (2.14), (3.1) can be considered as a supervised ELBO with an extra term  $p_\theta(y_i|z_i)$  that essentially formulates a regression of  $y_i$  with respect to  $z_i$ . Here we consider  $y_i$  as a continuous random variable, and set  $p_\theta(y_i|z_i)$  as a univariate Gaussian,  $p_\theta(y_i|z_i) \sim N(z_i^\top \beta + b, \sigma^2)$ , where  $\beta, \sigma^2 \in \theta$  are parameters that can be learned.

Similar to Section 2.2.2, we form the Monte Carlo estimate of  $\mathcal{L}(A_i, y_i; \theta, \phi)$  as

$$\mathcal{L}(A_i, y_i; \theta, \phi) \simeq \tilde{\mathcal{L}}(A_i, y_i; \theta, \phi) = -\frac{1}{L} \sum_{\ell=1}^L (\log p_\theta(A_i|z_i^\ell) + \log p_\theta(y_i|z_i^\ell)) + \frac{1}{2} \sum_{k=1}^K (\mu_k^2 + \sigma_k^2 - 1 - \log(\sigma_k^2)),$$

and estimate  $\theta, \phi$  following the stochastic variational Bayesian Algorithm 1 by replacing  $\tilde{\mathcal{L}}(A_i; \theta, \phi)$  with  $\tilde{\mathcal{L}}(A_i, y_i; \theta, \phi)$ . Figure 4 shows the flowchart of the reGATE architecture.

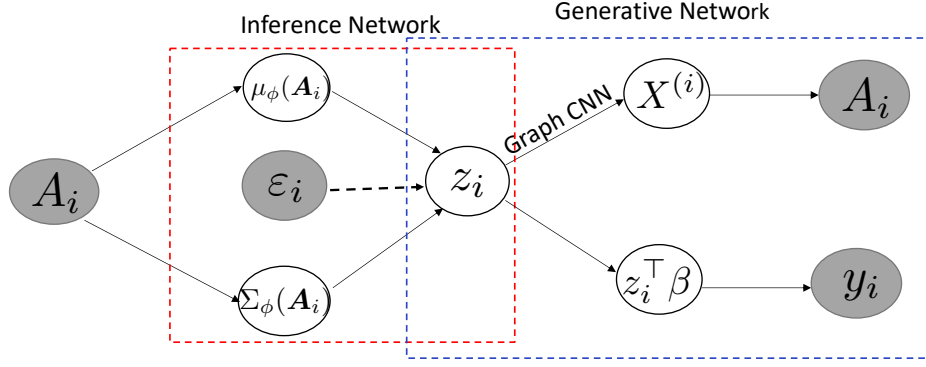


Figure 4: reGATE to predict the human trait. The dashed line with an arrow denotes a sampling operation.

### 3.2 Conditional generative model

In addition to prediction of human traits from their brain networks, we are also interested in inferring the distribution of brain networks given a covariate. For example, if  $y_i$  measures a person’s memory ability, we are interested in studying the difference in the distribution of brain networks between people with good and bad memory skills. More specifically, we are interested in performing inference of  $A_i$  given  $y_i$  via the generative mechanism inherited from the VAE. To achieve this goal, for each  $y_i$ , we need to learn  $p_\theta(z_i|y_i)$  and  $p_\theta(A_i|z_i)$ , where the latter is learned via the inference model in reGATE. Recall  $p_\theta(z_i) \sim N(0, I_K)$ , and  $p_\theta(y_i|z_i) \sim N(z_i^\top \beta + b, \sigma^2)$ . The posterior distribution of  $z_i$  given  $y_i$  has an explicit expression as follows:

$$\begin{aligned}
 p(z_i|y_i) &\propto p(y_i|z_i)p(z_i) \\
 &\propto \exp \left\{ -\frac{(y_i - z_i^\top \beta - b)^2}{2\sigma^2} - \frac{z_i^\top z_i}{2} \right\} \\
 &\propto \exp \left\{ -\frac{z_i^\top z_i + z_i^\top \beta \beta^\top z_i / \sigma^2 - 2z_i^\top \beta (y_i - b) / \sigma^2}{2} \right\} \\
 &\propto \exp \left\{ -\frac{z_i^\top (I_R + \beta \beta^\top / \sigma^2) z_i - 2z_i^\top \beta (y_i - b) / \sigma^2}{2} \right\}.
 \end{aligned}$$

Therefore, we have  $p_\theta(z_i|y_i) \sim N(\mu_z(y_i), \Sigma_z(y_i))$ , where

$$\mu_z(y_i) = (I_R + \beta \beta^\top / \sigma^2)^{-1} \beta (y_i - b) / \sigma^2, \quad \text{and} \quad \Sigma_z(y_i) = (I_R + \beta \beta^\top / \sigma^2)^{-1}. \quad (3.2)$$

Then the posterior computation of  $A_i$  given a particular  $y_i$  can be achieved by Gibbs sampling: update  $z_i$  from  $p_\theta(z_i|y_i)$  defined in (3.2), then update  $A_i$  from  $p_\theta(A_i|z_i)$ .

The latent representation  $z_i$  is unidentifiable in VAE. The log-likelihood and ELBO are rotationally invariant for  $z_i$ . For example, letting  $\tilde{z}_i = U^\top z_i$ , then  $P_{U,\theta}(A_i) = P_\theta(A_i)$  and

$$D_{KL}(q_{U,\phi}(z_i|A_i)||p_{U,\theta}(z_i|A_i)) = D_{KL}(q_\phi(z_i|A_i)||p_\theta(z_i|A_i)),$$

where  $U$  is an orthogonal matrix,  $q_{U,\phi}(\cdot)$  and  $p_{U,\theta}(\cdot)$  are defined by replacing  $z_i$  with  $\tilde{z}_i$  in  $q_\phi(\cdot)$  and  $p_\theta(\cdot)$ . Rotational invariance can be solved by post-processing to rotationally align the  $z_i$ 's. However, this would only be necessary if one is attempting to compare  $z_i$ s from different datasets or analyses of a given dataset. Within an analysis, the main focus is on inference on the relative values of  $z_i$ s, and these relative values are well defined. In addition, when the focus is on relating brain structure to human traits or in predicting traits based on brain structure or vice versa, the non-identifiability issue does not present a problem.

## 4 Simulation Study

We conduct a simulation study to evaluate the performance of GATE and reGATE in accurately characterizing replicated networks and predicting human traits. We simulate from four network structures: sparse networks according to the model in [35], community structures under the model of [36], small-worldness from the model in [37], and scale free property from the model in [38]. We simulate 100 networks with  $V = 68$  nodes for each type by sampling their edges from conditional independent Bernoulli random variables given their corresponding structure-specific edge probability. Each structure-specific edge probability vector is carefully constructed to assign high probability to a subset of network configurations characterized by a specific property. Figure 5 displays some example networks we generated with the four different network structures.

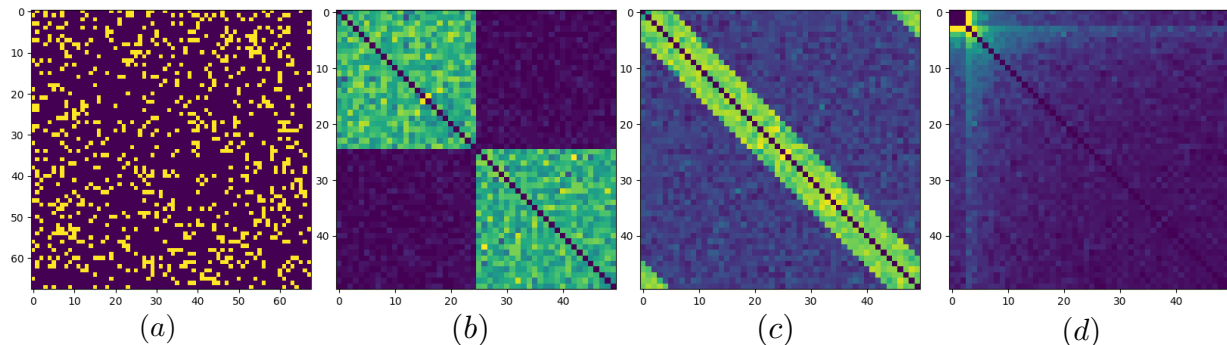


Figure 5: The edge probability vectors (rearranged in matrix form) from four network structures: (a) sparse graph, (b) community structure, (c) small world, (d) scale free.

We first generate  $y_i$  according to  $y_i = \alpha^\top A_i \alpha + \epsilon_i$ , where  $\alpha = (\underbrace{1, \dots, 1}_{17}, 0, \dots, 0)^\top \in \mathbb{R}^{68}$ , and  $\epsilon_i \sim N(0, 1)$ . We then standardize  $y_i$ , so that it ranges from  $-1.5$  to  $2.0$ . These settings aim to generate separable  $y_i$ 's according to the topological structures of  $A_i$ . The histograms in Figure 7 clearly demonstrate how  $y_i$  varies for different network structures. Our goals in this simulation study include (1) learning the latent representation under both the GATE and reGATE model; (2) inferring how the network connectivity structure varies with  $y_i$ ; (3) assessing the predictive performance of the reGATE model.

We train GATE and reGATE to obtain low-dimensional representations  $z_i$ 's. We then conduct PCA analysis on the posterior mean of  $z_i|A_i$  and plot the first two PC scores in  $\mathbb{R}^2$  colored with its corresponding  $y$  value. We can clearly observe the separation between these four types of networks in the low-dimensional representation space inferred using both GATE and reGATE model, with reGATE giving a more separable pattern.

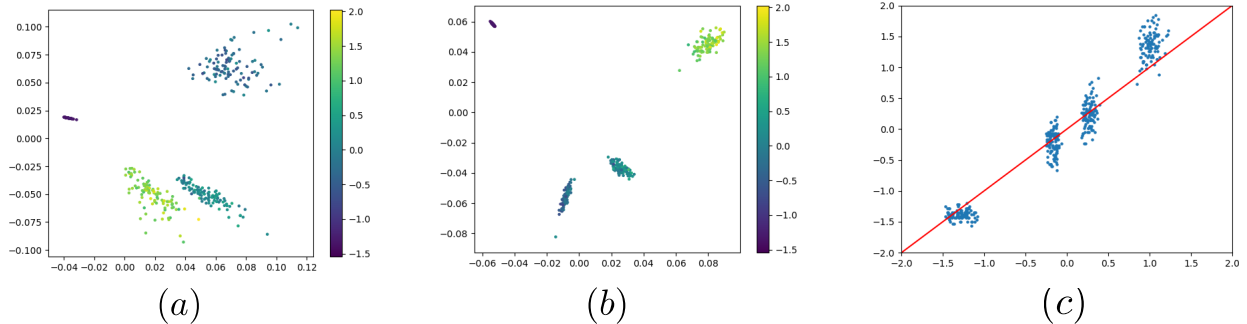


Figure 6: Plot of the first 2 PC scores of the posterior mean of  $z_i|A_i$  with corresponding  $y_i$ . Different colors refer to various values of  $y$ . (a) GATE, (b) reGATE. (c) Predicted  $y$  v.s. true  $y$  in reGATE, where x-axis is the true value and y-axis is the predicted value.

To infer how the network connectivity structure  $A_i$  varies according to  $y_i$ , we simulate networks by decoding the conditional mean of the latent generator  $p(z_i|y_i)$  for given  $y_i = (-1.5, -0.8, -0.1, 0.6, 2)$  with the previously trained reGATE. Then a mean network is calculated via a sequence of networks generated via  $p_\theta(A_i|z_i)$  for each  $y_i$ . Figure 7 shows the generated network with structure varying for different  $y_i$ 's. We can clearly observe that the mean network shows a sparse structure when  $y_i = -1.5$ , a mixture of sparse and community structure when  $y_i = -0.8$ , a mixture of community and small-world structure when  $y_i = -0.1$ , a mixture of community and small-world structure but with a more obvious small-world pattern when  $y_i = 0.6$ , and a clear scale free structure when  $y_i = 2$ . These generated structures are consistent with the training networks in our simulations.

To assess our third goal, we evaluate the prediction accuracy of reGATE. We consider two



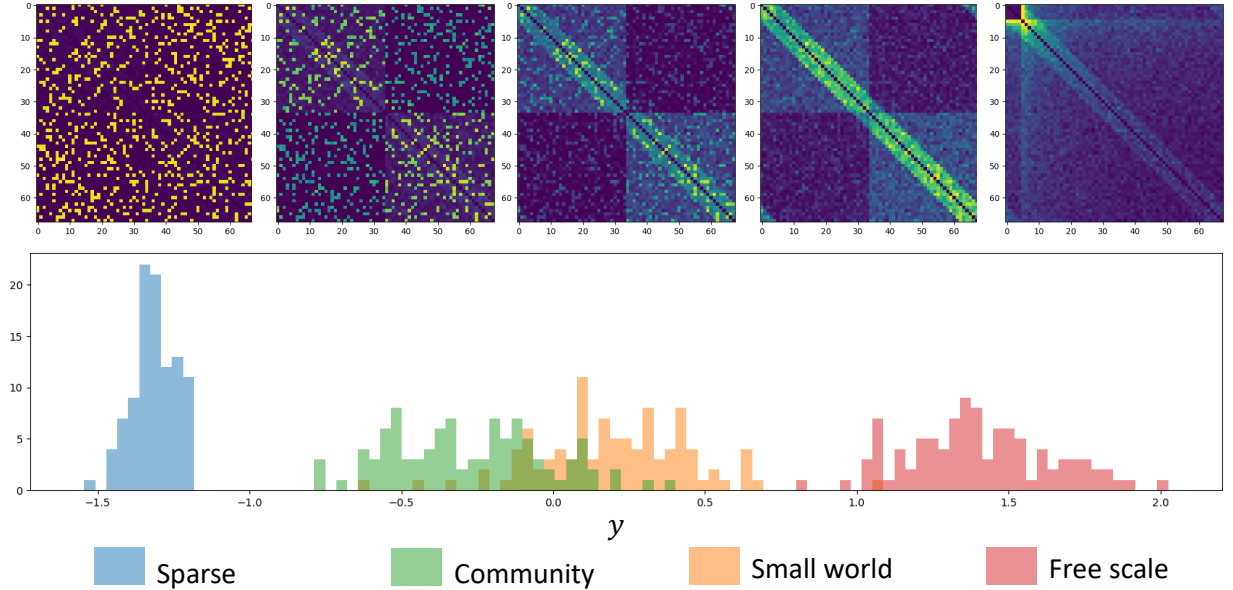


Figure 7: First row: generated networks conditional on the specific  $y_i$  using reGATE model, corresponding to  $y_i = -1.5, -0.8, -0.1, 0.6, 2$  respectively from left to right. Second row: histogram of  $y_i$  with respect to the network structure; x-axis is the value of  $y_i$ , y-axis is the frequency that belongs to a specific structure in the training data.

cases: (1)  $y_i = \alpha^\top A_i \alpha + \epsilon_i$ , which implies a linear relationship between  $y_i$  and  $A_i$ ; (2)  $y_i = (\alpha^\top A_i \alpha)^2 + (\alpha^\top A_i \alpha)^3 + \epsilon_i$ , which implies a nonlinear relationship between  $y_i$  and  $A_i$ . We also compare reGATE with a few popular methods in the literature for predicting human traits using network data. The first method is a regular linear regression based on tensor network principal component analysis (LR-TNPCA) in [17]. The second method is linear regression based on a regular PCA of the vectorized networks. The third method is tensor regression proposed in [39], denoted as CPR here. The mean square error (MSE) from five-fold cross validation was used to compare different approaches. Figure 6 (c) shows the association between the predicted value and the true value under the reGATE approach in case (1). The first and second row in Table 2 show the MSE under different methods. We can see reGATE outperforms other methods in predictive accuracy. The third row in Table 2 reports the computing time with 100 replicated simulations. reGATE is fast and powerful model, which not only has good prediction ability but also provides a well defined generative probabilistic model for further inference purposes.

We summarize the computing details used in the simulation study here. We run stochastic gradient descent with momentum (Adam [40]) on GATE and reGATE with learning rate 0.001 on 2 NVIDIA Titan-V GPU. In GATE, we use a batch size of 128, sampled uniformly at random at each

	reGATE	LR-TNPCA	LR-PCA	CPR
MSE: case 1	0.0252	0.0271	0.0340	0.0388
MSE: case 2	0.0505	0.0593	0.0700	0.1078
Time (mins)	17.5	197.6	5.3	253.7

Table 2: The first row and the second row are the MSE under different methods. The third row is the computing time based on 100 replications.

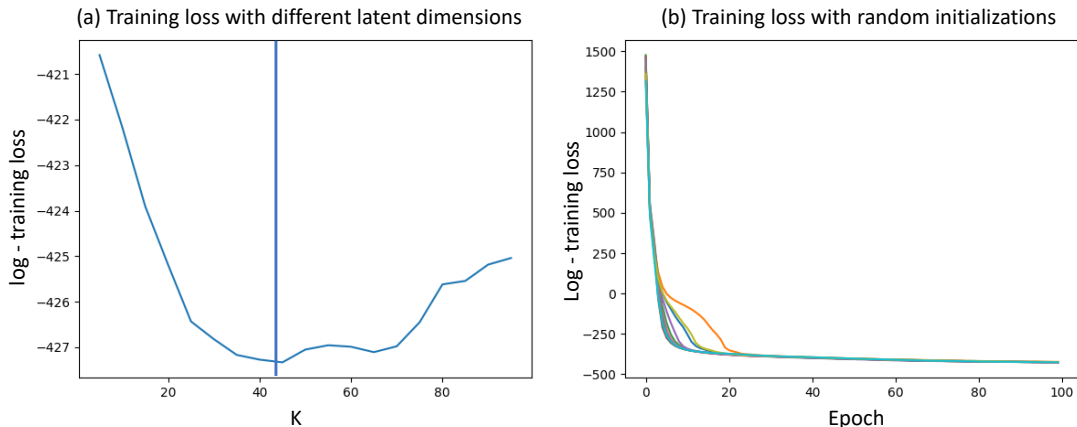


Figure 8: (a) log-training loss with latent dimension  $K$  varies; (b) the paths of the log-training loss with random initializations.

epoch and repeated for 1000 epochs. In reGATE, we use 5-fold CV to calculate the MSE, and ran 200 epochs with batch size of 128 for each training dataset. The experimental details and network architectures for the inference model and generative model training are summarized in Table 3. The latent dimension  $K$  is chosen as the smallest value that achieves the minimal training loss, provided that the network architectures are fixed as in Table 3. Figure 8 (a) shows the log-training loss with latent dimensions  $K$  varying from 5 to 100, and the training loss achieves the best performance when  $K$  is around 45. The sensitivity of the training loss with respect to the random initialization is also explored. As shown in Figure 8 (b), under different initializations, the paths of the training loss converges to the same level as the epoch increases.

	Inference model ( $\mu_\phi, \sigma_\phi$ )		Generative model	
	$\mu_\phi$ ( $N = 2$ )	$\sigma_\phi$ ( $N = 2$ )	setting	activation
GATE/reGATE ( $K = 45$ )	$W_{1,\mu} : 45 * 400$ $W_{2,\mu} : 400 * 45$ $b_{1,\mu} : 400 * 1$ $b_{2,\mu} : 45 * 1$ $\varphi_{1,\mu} = \text{ReLu}$ $\varphi_{2,\mu} = \text{Linear}$	$W_{1,\sigma} : 45 * 400$ $W_{2,\sigma} : 400 * 45$ $b_{1,\sigma} : 400 * 1$ $b_{2,\sigma} : 45 * 1$ $\varphi_{1,\sigma} = \text{Relu}$ $\varphi_{2,\sigma} = \text{Linear}$	$k\text{-NN}: 16$ $M = 2$ $R = 5$	$h_1: \text{Sigmoid}$ $h_2: \text{Sigmoid}$

Table 3: Experimental details and network architectures.  $K$  is the dimension of  $z_i$ ,  $N$  is the number of layers in the inference network,  $M$  is the number of layers in GCN,  $R$  is the dimension of  $X^{(i)}$ .

## 5 Human Connectome Project (HCP) Analysis

We apply our methods to the HCP dataset. The HCP aims at characterizing human brain connectivity in about 1,200 healthy adults and to enable detailed comparisons between brain circuits, behavior and genetics at the level of individual subjects [41]. Customized scanners were used to produce high-quality and consistent data to measure brain connectivity. The latest release containing various traits and MRI data can be easily accessed through ConnectomeDB. HCP also includes a test-retest dataset - a subset of HCP participants were recruited to undergo the full 3T HCP imaging and behavioral protocol for a second time. The rich trait data and high-resolution MRI data make the HCP dataset ideal for studying relationships between connectomes and human traits.

To reconstruct brain structural connectivity, we utilized a reproducible probabilistic tractography algorithm [42, 43] to generate the whole-brain tractography data for each subject in HCP. The method borrows anatomical information from high-resolution T1-weighted imaging to reduce bias in reconstruction. In the generated tractography data, each streamline has a step size of 0.2 mm. On average,  $10^5$  voxels were identified as the seeding region (white matter and gray matter interface region) for each individual in the HCP data set (with isotropic voxel size of 1.25 mm). For each seeding voxel, we initialized 16 streamlines to generate about  $10^6$  streamlines for each subject. We used the popular Desikan-Killiany atlas [44] to define ROIs corresponding to the nodes in the structural connectivity network. The Desikan-Killiany parcellation has 68 cortical surface regions with 34 nodes in each hemisphere. Freesurfer software [45, 46] is used to perform brain registration and parcellation. With the parcellation of an individual brain, we extract the number of fibers connecting two ROIs to generate the structural connectivity matrix  $A_i$ .

HCP uses a reliable and well-validated battery of measures that assess a wide range of human

functions, which are called traits in this paper. The core of this battery is comprised of the tools and methods developed by the NIH Toolbox for Assessment of Neurological and Behavioral function [47]. The Toolbox includes measures of cognitive, emotional, motor and sensory processes in healthy individuals. Since we are particularly interested in cognition, we extract four cognition related measures as  $y$  in our study, including (a) oral reading recognition test score, (b) picture vocabulary test score, (c) line orientation - total number correct, and (d) line orientation - total positions off for all trials. Oral reading and picture vocabulary tests measure language decoding skill and vocabulary knowledge. The two line orientation measures spatial orientation skill.

## 5.1 Data visualization

Both GATE and reGATE output low-dimensional representations of the brain networks. We would like to visualize the latent features of each individual’s connectome, and examine the relationship between the structural connectivity and the four traits via the latent features. We train GATE on 1065 brain networks extracted from HCP to obtain low-dimensional representations  $z_i$ . We then conduct PCA on the posterior mean of  $z_i|A_i$  and plot the first three PC scores in  $\mathbb{R}^3$  colored with its corresponding trait score. For each cognition trait, we only plot 200 subjects’ data, 100 subjects with low trait scores and 100 subjects with high scores. As shown in Figure 9 (a) – (d), under both GATE and reGATE, we can distinguish a separation between the two groups of subjects, indicating that brain connection patterns are different for the two groups. However, we highlight that the learned latent representation via reGATE is more informative about the trait, since we incorporate the trait information in learning  $z_i$ .

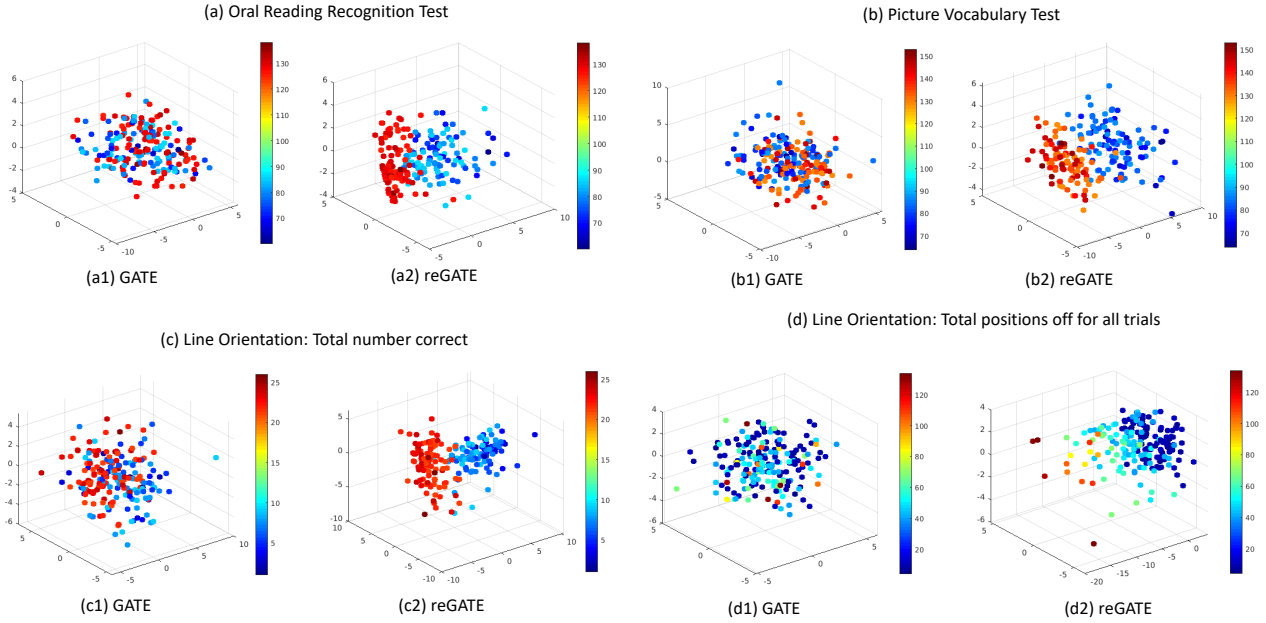


Figure 9: Brain PC scores under GATE and reGATE. For each trait, we selected 100 subjects with low trait scores and 100 subjects with high scores. Colors represent the trait scores.

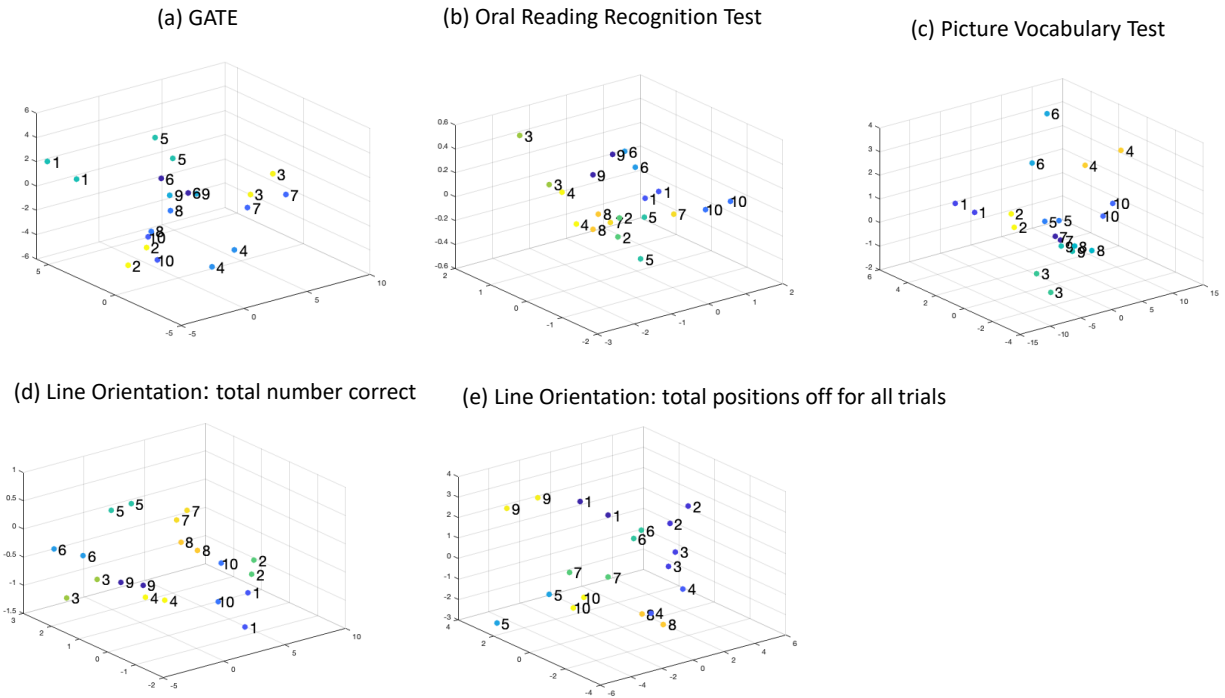


Figure 10: Brain PC scores from the HCP test-retest data set under GATE and reGATE with four different traits. Each unique combination of color represents two scans from the same subject.

We also apply GATE and reGATE to the HCP test-retest data. Figure 10 shows 10 selected subjects, with each unique combination of color and number representing two scans from the same subject. For both unsupervised GATE and supervised reGATE, the test-retest brain networks display a clear clustering pattern, implying that brain networks extracted from repeated scans are reproducible, and we can distinguish between different subjects based on the embedded feature  $z_i$ .

## 5.2 Goodness-of-fit via posterior predictive checks

Assessing the performance of a statistical model in recovering the generative mechanism underlying the observed data is fundamental to avoid poor characterizations, leading to substantially biased inference and conclusions. Therefore, model assessment is important to evaluate the model adequacy by comparing selected network summary measures computed for the observed data, with their distribution induced by the statistical model of interest. We here assess the performance of GATE in characterizing the observed brain network data from HCP via posterior predictive checks ([48]) for relevant network topological properties, including network density, mean eigencentality and average path length. In particular, we calculate the posterior predictive distributions for these measures based on the generative model  $p_\theta(A_i|z_i)$  in Section 2.2.1. Figure 11 compares the network summary measures computed using all 1065 subjects from the HCP data set (white colored) and the generated network data (gray colored) from our GATE model. Our model achieves good performance in characterizing the observed network summary measures, compared with the observed data.

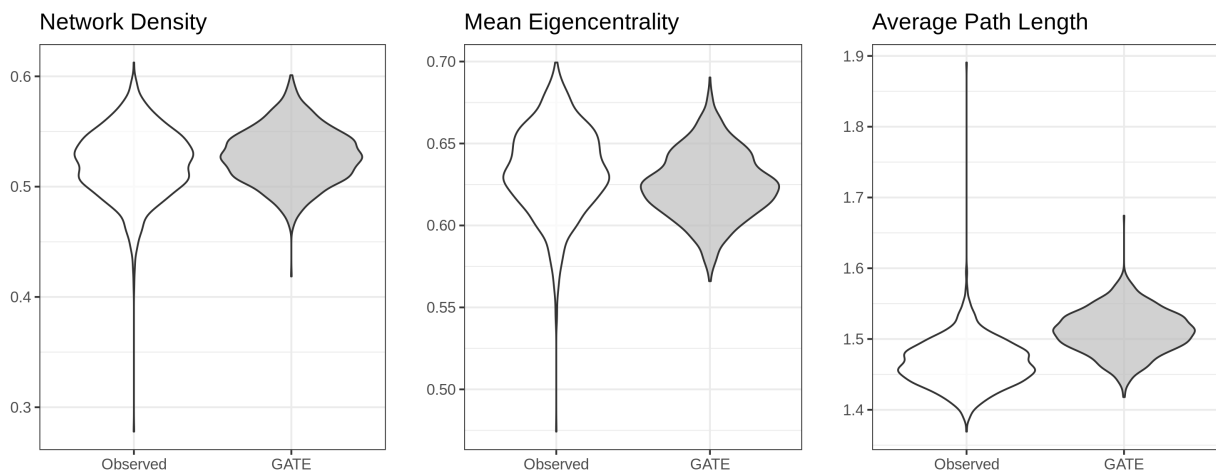


Figure 11: Goodness-of-fit assessments for selected network summary measures. The violin plots summarize the distribution in the observed data (white), and the posterior predictive distribution arising from GATE (gray).

### 5.3 Inference: generate the brain connectomes conditioned on traits

In this part, we focus on inferring how the brain network varies across different levels of  $y$  (trait). For each trait, we consider four levels that range from the minimal value to the maximum value, and generate the networks given that particular trait value. For example, in the oral reading recognition score, we consider  $y = 60, 91, 107$  and  $138$ . To make the comparison visualization more clear, we further dichotomize the connectome strength to 0, 1 depending on whether the connection strength is 0 or not. For each  $y$ , we generate a mean network via the conditional generative procedure in Section 3.2. These generated networks are shown in Figure 12, where the first row of each panel shows generated networks (with the first 34 nodes from the left side of the brain and the next 34 nodes from the right side of the brain), and the second row shows the distribution of the traits. From (a), we can clearly see the difference among the connections between left and right brains from lower reading score to high reading score, indicating that a richer connection between two hemispheres of the brain is correlated to better reading ability. Similarly, we observe such phenomena in Figure 12 (b)-(d) for different traits. This result is consistent with findings in the literature [49, 16].

In addition to exploring the association between traits and connectomes, we examine how the association changes specific to certain subnetwork and the direction of these associations. For a given trait, we select the 25%th and 75%th quantile from the observation  $\{y_i\}_{i=1}^n$  as two representative levels. For each level, we generate 100 conditional networks and calculate the mean difference between the two groups of networks. Figure 13 plots the top 50 connections (separated by positive and negative ones) in the mean difference network for the three cognition-related traits. From an initial glance at these difference maps, we observe that (1) the top 50 connections are dominated by positive ones, indicating that richer connections are associated with better cognitive traits; and (2) the positive ones are dominated by cross-hemisphere connections, especially connections with weights  $> 1000$ .

In the oral reading test, participants were asked to read and pronounce letters and words as accurately as possible. The difference map generated by the oral reading test shows that the connections  $(r29, r32)$ ,  $(l16, r16)$ ,  $(l16, r29)$ ,  $(l27, r27)$  stand out with significantly high weights. These connections include regions such as superior temporal gyrus (29), temporal pole (32), paracentral lobule (16) and superior frontal gyrus (27). The superior temporal gyrus includes the auditory cortex, which processes sounds; the right temporal pole is related to episodic memories [50]; the paracentral lobe controls motor and sensory; and the superior frontal gyrus contributes to high cognitive functions and particularly to working memory [51]. We notice that this is a subnetwork that integrates motion, audio, high cognition and working memory, which are essential to performing the oral reading test. This is therefore consistent with the interpretation that stronger anatomical wiring between brain regions that contribute to audition, motion, higher cognitive functions and working



memory is associated with improved performance on this task. We observe better picture vocabulary test performance to be associated with stronger left and right superior frontal gyrus connection. In the picture vocabulary test, participants were presented with an audio recording of a word and four photographic images on the computer screen and were asked to select the picture that most closely matches the meaning of the word. Higher cognitive functions and better episodic memory are essential to this task. In the line orientation test, two line segments were presented on the screen and participants were asked to rotate a movable line to make it parallel to the fixed line. Here we identify a subnetwork consisting of connections of  $(l16, r16)$ ,  $(l16, l31)$ ,  $(l30, r30)$ ,  $(l5, r5)$ ,  $(l17, r2)$ , showing significantly higher weights. This subnetwork includes the paracentral lobule involved in sensory motor control, the supramarginal gyrus (indexed as ROI 30), involved in the interpretation of tactile sensory data and in the perception of space and limbs location, the entorhinal cortex (indexed as ROI 5) involved in navigation [52], brodmann area 10 (indexed as 31) involved in executive functions, and the anterior cingulate cortex (indexed as ROI 2) involved in error detection, attention and negative affect [53].

Some negative connections within each hemisphere are also observed, although both their numbers and strengths are smaller than the positive ones. One possible explanation of these observations is that the fibers of these within hemisphere connections are easier to generate and are much more susceptible to emerge as false positives using existing tractography algorithms. It is possible that these connections arise from errors introduced during the connection recovery stage. Another possible explanation is that fewer connections between these brain regions indeed help with these cognitive tasks. However, both explanations need future validation and study.

#### 5.4 Prediction of traits with reGATE

We examine the predictive accuracies of reGATE, and compare with LR-TNPCA [17], LR-PCA, CPR [39], and BLR [54]. BLR is the supervised bi-linear regression (BLR) with emphasis on signal sub-network selection. The mean square error (MSE) from five-fold CV is used to assess the performance. Table 4 shows the comparison result. We can see that our proposed reGATE outperforms other methods in all of the four traits.

#### 5.5 Network architecture summary

We summarize the computing details used in Section 5. We run Adam on GATE and reGATE with learning rate 0.001 on 2 NVIDIA Titan-V GPU. In GATE, we used a batch size of 128 sampled uniformly at random at each epoch and ran 200 epochs. In reGATE, we used 5-fold CV to calculate the MSE, and ran 100 epochs with batch size of 128 for each training dataset. The latent dimension

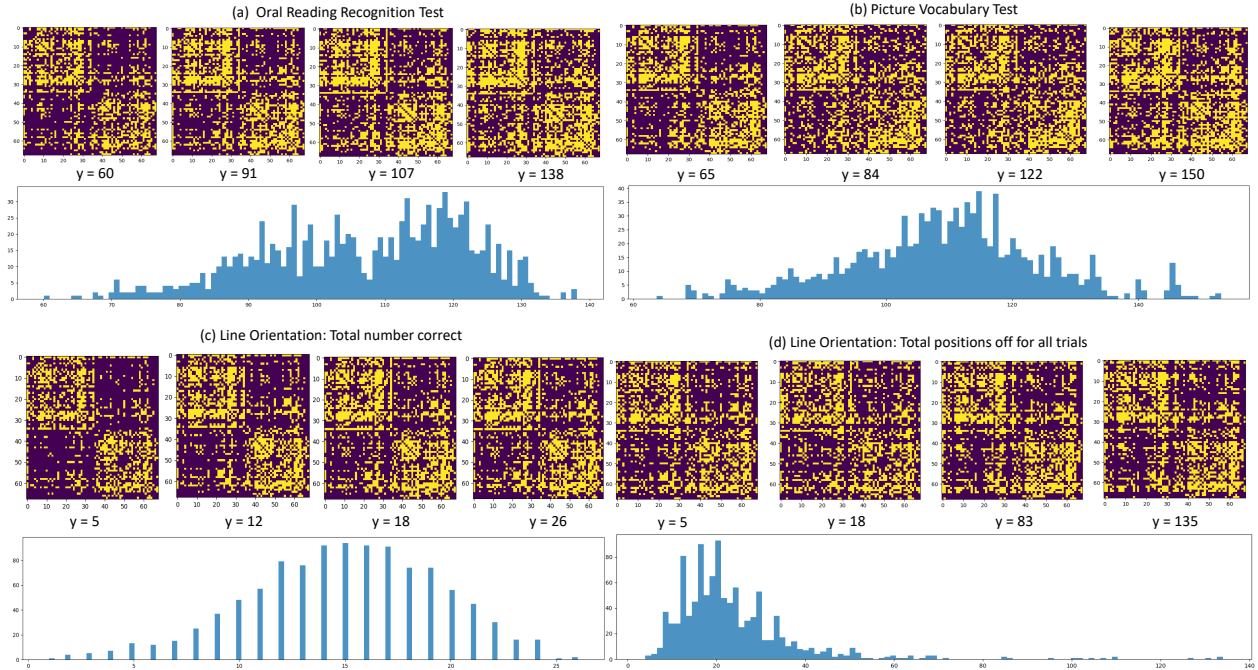


Figure 12: First row in (a)-(d): generated brain connectomes conditional on different levels of four traits under the reGATE model. Second row in (a)-(d): histogram of the observed scores with different traits for the 1065 individuals.

Trait	reGATE	LR-TNPCA	LR-PCA	CPR	BLR
Oral Reading Recognition Test	198.9	202.1	204.2	252.1	200.4
Picture Vocabulary Test	209.1	214.5	219.0	257.2	216.1
Line Orientation: Total number correct	17.8	18.5	18.2	21.9	18.8
Line Orientation: Total positions off for all traits	195.8	201.8	202.6	259.0	200.7

Table 4: MSE for trait prediction using different methods calculated via five-fold CV.

$K$  can be chosen as 68 under the same criteria as in Section 4. Table 5 shows the detailed network architectures for the inference model and generative model training.

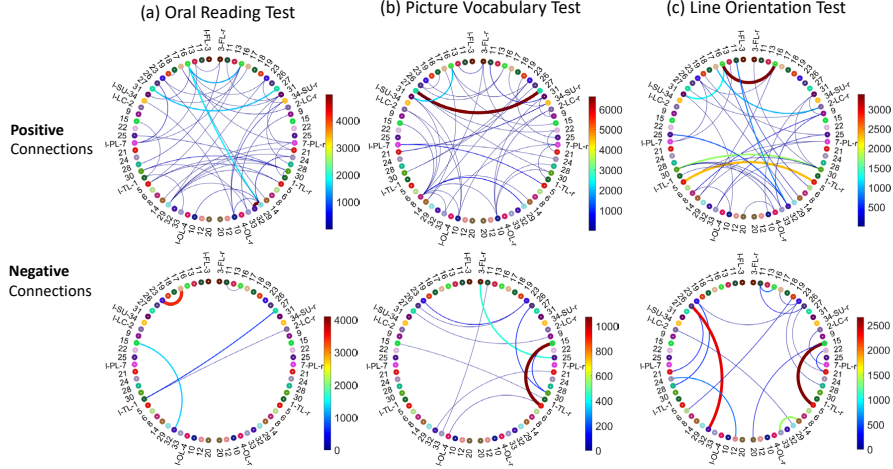


Figure 13: Top 50 pairs of brain regions in terms of the mean changes in the generated brain connectivity with different level of traits. The first row shows the positive connections among the 50 pairs and the second row shows negative connections.

	Inference model $(\mu_\phi, \sigma_\phi)$		Generative model	
	$\mu_\phi (N = 2)$	$\sigma_\phi (N = 2)$	setting	activation
GATE/reGATE ( $K = 68$ )	$W_{1,\mu} : 68 * 256$	$W_{1,\sigma} : 68 * 256$	$k$ -NN: 32 $M = 2$ $R = 5$	$h_1$ : Sigmoid $h_2$ : Sigmoid
	$W_{2,\mu} : 256 * 68$	$W_{2,\sigma} : 256 * 68$		
	$b_{1,\mu} : 256 * 1$	$b_{1,\sigma} : 256 * 1$		
	$b_{2,\mu} : 68 * 1$	$b_{2,\sigma} : 68 * 1$		
	$\varphi_{1,\mu} = \text{Relu}$	$\varphi_{1,\sigma} = \text{Relu}$		
	$\varphi_{2,\mu} = \text{Linear}$	$\varphi_{2,\sigma} = \text{Linear}$		

Table 5: Experimental details and network architectures.  $K$  is the dimension of  $z_i$ ,  $N$  is the number of layers in the inference network,  $M$  is the number of layers in GCN,  $R$  is the dimension of  $X^{(i)}$ .

## 6 Discussion

We develop a novel nonlinear latent factor model to characterize the population distribution of replicated graphs, providing procedures for coherent and flexible inference of network data. GATE outputs two layers of low dimensional nonlinear latent representations: one on the individuals that can be used as a summary score for visualization and prediction of human traits of interest; and one on the nodes for characterizing the network structure of each individual based on a latent space model. GATE/reGATE is developed based on a deep neural network framework and implemented via stochastic variational Bayesian algorithm. Therefore, it is computationally efficient, and can be

easily extended to massive networks with very large number of nodes.

With an application to the HCP data, we use GATE and reGATE to study the relationship between brain structural connectomes and various cognition measures. Using the generative model of reGATE, we are able to simulate brain networks for a given  $y$  (e.g., cognition measure); we then compare these brain networks generated by different  $y$ 's. For these cognition traits we clearly observe that, cross hemispheres connections are critical. In addition to simulating brain network data, reGATE is also a winner in terms of predicting trait scores from brain networks. With the availability of larger brain imaging datasets, such as the UK Biobank [5] (with  $> 20,000$  subjects) and the Adolescent Brain Cognitive Development study [7] (with  $> 10,000$ ) subjects, we expect even better of GATE performance and reGATE model.

In the future, we would like to extent GATE/reGATE in the following directions. First, in brain networks, a refined division of the brain can give a larger number of nodes, providing a more detailed description of the brain. Previous MCMC based inference framework has difficulties to handle such large-scale multi-networks. GATE and reGATE provides a set of new tools in this scenario. Moreover, current large datasets all collect both functional MRI and diffusion MRI data. We now have opportunities to study the collaborative pattern between these two different connectomes, leveraging the effectivity and efficiency of GATE and reGATE.

## References

- [1] Hae-Jeong Park and Karl Friston. “Structural and functional brain networks: from connections to cognition”. In: *Science* 342.6158 (2013), p. 1238411.
- [2] Alex Fornito, Andrew Zalesky, and Michael Breakspear. “Graph analysis of the human connectome: promise, progress, and pitfalls”. In: *NeuroImage* 80 (2013), pp. 426–444.
- [3] R Cameron Craddock, Saad Jbabdi, Chao-Gan Yan, Joshua T Vogelstein, F Xavier Castellanos, Adriana Di Martino, Clare Kelly, Keith Heberlein, Stan Colcombe, and Michael P Milham. “Imaging human connectomes at the macroscale”. In: *Nature Methods* 10.6 (2013), pp. 524–539.
- [4] D. K. Jones, T. R. Knosche, and R. Turner. “White matter integrity, fiber count, and other fallacies: the do’s and don’ts of diffusion MRI”. In: *NeuroImage* 73 (2013), pp. 239–254.
- [5] Karla L Miller, Fidel Alfaro-Almagro, Neal K Bangerter, David L Thomas, Essa Yacoub, Junqian Xu, Andreas J Bartsch, Saad Jbabdi, Stamatios N Sotiropoulos, and Jesper LR Andersson. “Multimodal population brain imaging in the UK Biobank prospective epidemiological study”. In: *Nature Neuroscience* 19.11 (2016), p. 1523.

- [6] David C Van Essen, Stephen M Smith, Deanna M Barch, Timothy EJ Behrens, Essa Yacoub, Kamil Ugurbil, and Wu-Minn HCP Consortium. “The WU-Minn human connectome project: an overview”. In: *NeuroImage* 80 (2013), pp. 62–79.
- [7] BJ Casey, Tariq Cannonier, May I Conley, Alexandra O Cohen, Deanna M Barch, Mary M Heitzeg, Mary E Soules, Theresa Teslovich, Danielle V Dellarco, and Hugh Garavan. “The adolescent brain cognitive development (ABCD) study: imaging acquisition across 21 sites”. In: *Developmental Cognitive Neuroscience* (2018).
- [8] Matthew F Glasser, Stephen M Smith, Daniel S Marcus, Jesper LR Andersson, Edward J Auerbach, Timothy EJ Behrens, Timothy S Coalson, Michael P Harms, Mark Jenkinson, and Steen Moeller. “The human connectome project’s neuroimaging approach”. In: *Nature Neuroscience* 19.9 (2016), pp. 1175–1187.
- [9] D. S. Tuch. “Q-ball imaging”. In: *Magn Reson Med* 52.6 (2004), pp. 1358–1372.
- [10] Zhengwu Zhang, Maxime Descoteaux, Jingwen Zhang, Gabriel Girard, Maxime Chamberland, David Dunson, Anuj Srivastava, and Hongtu Zhu. “Mapping Population-based Structural Connectomes”. In: *NeuroImage* 172 (2018), pp. 130–145.
- [11] R. E. Smith, J. D. Tournier, F. Calamante, and A. Connelly. “Anatomically-constrained tractography: improved diffusion MRI streamlines tractography through effective use of anatomical information”. In: *NeuroImage* 62.3 (2012), pp. 1924–1938.
- [12] Daniele Durante, David B Dunson, and Joshua T Vogelstein. “Nonparametric Bayes modeling of populations of networks”. In: *Journal of the American Statistical Association* 112.520 (2017), pp. 1516–1530.
- [13] Edoardo M Airoldi, David M Blei, Stephen E Fienberg, Eric P Xing, and Tommi Jaakkola. “Mixed membership stochastic block models for relational data with application to protein-protein interactions”. In: *Proceedings of the International Biometrics Society Annual Meeting*. Vol. 15. 2006.
- [14] Peter D Hoff, Adrian E Raftery, and Mark S Handcock. “Latent space approaches to social network analysis”. In: *Journal of the American Statistical Association* 97.460 (2002), pp. 1090–1098.
- [15] Daniele Durante, David B Dunson, and Joshua T Vogelstein. “Nonparametric Bayes modeling of populations of networks”. In: *Journal of the American Statistical Association* 112.520 (2017), pp. 1516–1530.
- [16] Daniele Durante and David B Dunson. “Bayesian inference and testing of group differences in brain networks”. In: *Bayesian Analysis* 13.1 (2018), pp. 29–58.

- [17] Zhengwu Zhang, Genevera I Allen, Hongtu Zhu, and David Dunson. “Tensor network factorizations: Relationships between brain structural connectomes and traits”. In: *NeuroImage* (2019).
- [18] Lu Wang Zhengwu Zhang and David Dunson. “Common and individual structure of multiple networks”. In: *The Annals of Applied Statistics* 13.1 (2019), pp. 85–112.
- [19] Diederik P Kingma and Max Welling. “Auto-encoding Variational Bayes”. In: *In International Conference on Learning Representations* (2014).
- [20] Danilo Jimenez Rezende, Shakir Mohamed, and Daan Wierstra. “Stochastic backpropagation and approximate inference in deep generative models”. In: *In International Conference on Machine Learning* (2014), pp. 1278–1286.
- [21] Alex Krizhevsky, Ilya Sutskever, and Geoffrey E Hinton. “Imagenet classification with deep convolutional neural networks”. In: *Advances in Neural Information Processing Systems*. 2012, pp. 1097–1105.
- [22] Pierre Sermanet, Soumith Chintala, and Yann LeCun. “Convolutional neural networks applied to house numbers digit classification”. In: *In International Conference on Pattern Recognition (ICPR 2012)* (2012).
- [23] Geoffrey Hinton, Li Deng, Dong Yu, George Dahl, Abdel-rahman Mohamed, Navdeep Jaitly, Andrew Senior, Vincent Vanhoucke, Patrick Nguyen, and Brian Kingsbury. “Deep neural networks for acoustic modeling in speech recognition”. In: *IEEE Signal Processing Magazine* 29 (2012).
- [24] Michaël Defferrard, Xavier Bresson, and Pierre Vandergheynst. “Convolutional neural networks on graphs with fast localized spectral filtering”. In: *Advances in Neural Information Processing Systems*. 2016, pp. 3844–3852.
- [25] William L Hamilton, Rex Ying, and Jure Leskovec. “Representation learning on graphs: Methods and applications”. In: *arXiv preprint arXiv:1709.05584* (2017).
- [26] Thomas N Kipf and Max Welling. “Semi-supervised classification with graph convolutional networks”. In: *In International Conference on Learning Representations* (2017).
- [27] Joan Bruna, Wojciech Zaremba, Arthur Szlam, and Yann LeCun. “Spectral networks and locally connected networks on graphs”. In: *in Proceedings of International Conference on Learning Representations* (2014).
- [28] Mathias Niepert, Mohamed Ahmed, and Konstantin Kutzkov. “Learning convolutional neural networks for graphs”. In: *In International Conference on Machine Learning*. 2016, pp. 2014–2023.

- [29] YoungJoon Yoo, Sangdoon Yun, Hyung Jin Chang, Yiannis Demiris, and Jin Young Choi. “Variational autoencoded regression: high dimensional regression of visual data on complex manifold”. In: *Proceedings of the IEEE Conference on Computer Vision and Pattern Recognition*. 2017, pp. 3674–3683.
- [30] Joel Jaskari and Jyri J Kivinen. “A Novel Variational Autoencoder with Applications to Generative Modelling, Classification, and Ordinal Regression”. In: *arXiv preprint arXiv:1812.07352* (2018).
- [31] Qingyu Zhao, Ehsan Adeli, Nicolas Honnorat, Tuo Leng, and Kilian M Pohl. “Variational AutoEncoder For Regression: Application to Brain Aging Analysis”. In: *arXiv preprint arXiv:1904.05948* (2019).
- [32] Ian Goodfellow, Yoshua Bengio, and Aaron Courville. *Deep learning*. MIT press, 2016.
- [33] Michael I Jordan, Zoubin Ghahramani, Tommi S Jaakkola, and Lawrence K Saul. “An introduction to variational methods for graphical models”. In: *Machine Learning* 37.2 (1999), pp. 183–233.
- [34] Matthew D Hoffman, David M Blei, Chong Wang, and John Paisley. “Stochastic variational inference”. In: *The Journal of Machine Learning Research* 14.1 (2013), pp. 1303–1347.
- [35] Donald B Johnson. “Efficient algorithms for shortest paths in sparse networks”. In: *Journal of the ACM (JACM)* 24.1 (1977), pp. 1–13.
- [36] Krzysztof Nowicki and Tom A B Snijders. “Estimation and prediction for stochastic block-structures”. In: *Journal of the American Statistical Association* 96.455 (2001), pp. 1077–1087.
- [37] Duncan J Watts and Steven H Strogatz. “Collective dynamics of small-world networks”. In: *Nature* 393.6684 (1998), p. 440.
- [38] Albert-László Barabási and Réka Albert. “Emergence of scaling in random networks”. In: *Science* 286.5439 (1999), pp. 509–512.
- [39] Hua Zhou, Lexin Li, and Hongtu Zhu. “Tensor regression with applications in neuroimaging data analysis”. In: *Journal of the American Statistical Association* 108.502 (2013), pp. 540–552.
- [40] Diederik P Kingma and Jimmy Ba. “Adam: A method for stochastic optimization”. In: *International Conference on Learning Representations (ICLR)* (2015).
- [41] David C Van Essen, Kamil Ugurbil, E Auerbach, D Barch, TEJ Behrens, R Bucholz, Acer Chang, Liyong Chen, Maurizio Corbetta, and Sandra W Curtiss. “The Human Connectome Project: a data acquisition perspective”. In: *NeuroImage* 62.4 (2012), pp. 2222–2231.



- [42] Gabriel Girard, Kevin Whittingstall, Rachid Deriche, and Maxime Descoteaux. “Towards quantitative connectivity analysis: reducing tractography biases”. In: *NeuroImage* 98 (2014), pp. 266–278.
- [43] Klaus H Maier-Hein, Peter F Neher, Jean-Christophe Houde, Marc-Alexandre Côté, Eleftherios Garyfallidis, Jidan Zhong, Maxime Chamberland, Fang-Cheng Yeh, Ying-Chia Lin, and Qing Ji. “The challenge of mapping the human connectome based on diffusion tractography”. In: *Nature Communications* 8.1 (2017), p. 1349.
- [44] Rahul S. Desikan, Florent Segonne, Bruce Fischl, Brian T. Quinn, Bradford C. Dickerson, Deborah Blacker, Randy L. Buckner, Anders M. Dale, R. Paul Maguire, Bradley T. Hyman, Marilyn S. Albert, and Ronald J. Killiany. “An automated labeling system for subdividing the human cerebral cortex on MRI scans into gyral based regions of interest”. In: *NeuroImage* 31.3 (2006), pp. 968–980.
- [45] Anders M Dale, Bruce Fischl, and Martin I Sereno. “Cortical surface-based analysis: I. Segmentation and surface reconstruction”. In: *NeuroImage* 9.2 (1999), pp. 179–194.
- [46] Bruce Fischl, David H. Salat, Andre J.W. van der Kouwe, Nikos Makris, Florent Segonne, Brian T. Quinn, and Anders M. Dale. “Sequence-independent segmentation of magnetic resonance images”. In: *NeuroImage* 23.Supplement 1 (2004), S69–S84.
- [47] Richard C. Gershon, Molly V. Wagster, Hugh C. Hendrie, Nathan A. Fox, Karon F. Cook, and Cindy J. Nowinski. “NIH Toolbox for Assessment of Neurological and Behavioral Function”. In: *Neurology* 80.11 (2013), S2–S6. ISSN: 0028-3878.
- [48] Andrew Gelman, John B Carlin, Hal S Stern, David B Dunson, Aki Vehtari, and Donald B Rubin. *Bayesian Data Analysis*. Chapman and Hall/CRC, 2013.
- [49] Ed Bullmore and Olaf Sporns. “Complex brain networks: graph theoretical analysis of structural and functional systems”. In: *Nature Reviews Neuroscience* 10.3 (2009), p. 186.
- [50] Katsuki Nakamura, Ryuta Kawashima, Motoaki Sugiura, Takashi Kato, Akinori Nakamura, Kentaro Hatano, Sumiharu Nagumo, Kisou Kubota, Hiroshi Fukuda, and Kengo Ito. “Neural substrates for recognition of familiar voices: a PET study”. In: *Neuropsychologia* 39.10 (2001), pp. 1047–1054.
- [51] Foucaud du Boisgueheneuc, Richard Levy, Emmanuelle Volle, Magali Seassau, Hughes Duffau, Serge Kinkingnehun, Yves Samson, Sandy Zhang, and Bruno Dubois. “Functions of the left superior frontal gyrus in humans: a lesion study”. In: *Brain* 129.12 (2006), pp. 3315–3328.
- [52] Torkel Hafting, Marianne Fyhn, Sturla Molden, May-Britt Moser, and Edvard I Moser. “Microstructure of a spatial map in the entorhinal cortex”. In: *Nature* 436.7052 (2005), p. 801.

- [53] José V Pardo, Patricia J Pardo, Kevin W Janer, and Marcus E Raichle. “The anterior cingulate cortex mediates processing selection in the Stroop attentional conflict paradigm”. In: *Proceedings of the National Academy of Sciences* 87.1 (1990), pp. 256–259.
- [54] Lu Wang, Zhengwu Zhang, and David B Dunson. “Symmetric Bilinear Regression for Signal Subgraph Estimation”. In: *IEEE Transactions on Signal Processing* 67 (7 2019), pp. 1929–1940.